

Fermion Scattering by a Schwarzschild Black Hole

Sam Dolan,^x Chris Doran,^y and Anthony Lasenby^z

Cavendish Laboratory,
University of Cambridge,
J J Thomson Avenue,
Cambridge CB3 0HE, UK

(Dated: March 1, 2022)

Abstract

We study the scattering of massive spin-half waves by a Schwarzschild black hole using analytical and numerical methods. We begin by extending a recent perturbation theory calculation to next order to obtain Born series for the differential cross section and Mott polarization, valid at small couplings. We continue by deriving an approximation for glory scattering of massive spinor particles by considering classical timelike geodesics and spin precession. Next, we formulate the Dirac equation on a black hole background, and outline a simple numerical method for finding partial wave series solutions. Finally, we present our numerical calculations of absorption and scattering cross sections and polarization, and compare with theoretical expectations.

PACS numbers: 04.70.Bw, 03.65.Nk, 04.30.Nk, 97.60.Lf

^xElectronic address: s.dolan@mrao.cam.ac.uk

^yElectronic address: c.doran@mrao.cam.ac.uk

^zElectronic address: a.n.lasenby@mrao.cam.ac.uk

I. INTRODUCTION

Scattering by gravitational sources has been an important test for General Relativity since its inception. An early success for Einstein's theory came with verification of the prediction that starlight is deflected as it passes close to the Sun. The experiments conducted by Eddington and his team during the solar eclipse of 1919 were important in establishing GR as a credible theory of gravitation. More recently, gravitational lensing observations provide a strong test of the theory, as well as information about lensing mass distributions and distant astronomical sources.

Gravitational scattering from astrophysical objects may be understood entirely in terms of geometric optics through the analysis of classical geodesics. Nevertheless, to obtain a deeper theoretical understanding of extreme objects such as black holes many authors have also considered the scattering of coherent waves. If the wavelength of the incident wave is comparable with the size of the event horizon then the wave will be diffracted by the black hole. Diffraction effects are responsible for many interesting phenomena in nature, such as glories and rainbows, so wave scattering from black holes is an interesting field in its own right, even if observations may not be realisable in practice.

In this paper, we study how quantum waves are scattered by a Schwarzschild black hole. This problem has been considered in numerous papers [1]–[14] and books [15, 16, 17]. Most authors study the massless scalar wave (with spin $s = 0$) for its mathematical simplicity, or massless electromagnetic ($s = 1$) and gravitational ($s = 2$) waves for physical relevance. In this paper, we focus instead on fermion scattering ($s = 1/2$), which has been less frequently discussed [16]. We investigate the effect of particle mass on scattering cross sections and polarization.

The interaction of an incident plane wave with a black hole may be understood in terms of three quantities: the total absorption cross section σ_A , the differential scattering cross section $d\sigma/d\Omega$, and the polarization P that is induced in initially unpolarized beam (note that $d\sigma/d\Omega$ and P are functions of the scattering angle θ). In this paper we calculate these quantities using a variety of analytical and numerical methods.

The paper is organised as follows. In section II we review classical scattering on the Schwarzschild background. We derive a new approximation for near-horizon deflection of timelike geodesics, and investigate classical spin precession on backward-scattering orbits.

In section III we describe analytic methods that can be applied to fermion scattering. The perturbation-theory approach introduced by Doran and Lasenby [14] is taken to the next order, which provides a new estimate of the cross section and polarization at low couplings. The glory-scattering approximation of Zhang and DeWitt-Morette [9] is extended to the massive case, employing the classical results of section II. In section IV we discuss partial wave scattering theory, formulate the Dirac equation, and outline a simple numerical method for calculating phase shifts. In section V we present the results of our numerical calculations, and compare with theory. We conclude in section VI by discussing the significance of our results and possible future work.

Note that in this article we employ units in which the speed of light (c), the gravitational constant (G), and Planck's constant over 2 (\hbar) are set to unity.

II. CLASSICAL SCATTERING

We begin by reviewing some results for classical scattering and absorption on a Schwarzschild background. We then investigate the precession of classical spin vectors along scattering trajectories. As well as being of interest in their own right, the results of this section will aid our interpretation of the wave scattering cross sections presented in section V. The results of this section are also required in section III to derive a new approximation for glory scattering of massive spinor waves.

The Schwarzschild spacetime is invariant under time-displacement and rotation. These symmetries imply the existence of Killing vectors, and the quantities conjugate to those Killing vectors are conserved along geodesics. That is, the particle energy E , and angular momentum L , are constants of motion.

The motion of a particle of rest mass m on a Schwarzschild background is described by the orbit equation

$$\left(\frac{du}{d\varphi}\right)^2 = 2M u^3 - u^2 + \frac{2M m^2}{L^2} u + \frac{E^2 - m^2}{L^2}; \quad (1)$$

where $u = 1/r$, and φ is the polar angle. For descriptive purposes it is useful to define three further constants: the momentum $p = (E^2 - m^2)^{1/2}$, the impact parameter $b = L/p$, and the speed $v = p/E$. At large distances from the hole, each has a simple physical interpretation: p is the incident particle momentum, b is the orthogonal distance to the scattering centre,

and v is the particle speed in units of c . Note that for null geodesics, $v = 1$ and $p = E$. With these definitions we may rewrite the orbital equation (1) as

$$\frac{du}{d\phi}^2 = 2M u^3 - u^2 + \frac{2M(1-v^2)}{v^2 b^2} u + \frac{1}{b^2} : \quad (2)$$

The unbound scattering solutions of (2) can be written in terms of elliptic integrals. For a comprehensive treatment, see Chandrasekhar [15].

A. Deflection-angle Approximations

In the weak-field limit, $r \gg 2M$, the deflection angle for timelike geodesics is approximately

$$\frac{2M(1+v^2)}{bv^2} : \quad (3)$$

For null geodesics we set $v = 1$ to recover the Einstein deflection angle for the bending of light, $4M/b$. In the strong-field regime, the above approximation underestimates the deflection; incoming geodesics may be scattered through large angles or even orbit the hole several times before escaping (see Fig. 1). Trajectories that make too close an approach to the hole spiral inwards, and end on the singularity. The last geodesic to avoid the singularity defines a critical impact parameter b_c . All geodesics with $b > b_c$ are scattered, whereas all geodesics with $b < b_c$ are absorbed. By considering the zeros of (2), one can show (see e.g. [18]) that

$$b_c = \frac{M}{\sqrt{8v^4 + 20v^2 - 1 + (1 + 8v^2)^{3/2 - 1/2}}} : \quad (4)$$

For null geodesics, the critical impact parameter is $b_c = \frac{3}{2}\sqrt{3}M$. The classical absorption cross section is simply the area of the circle defined by the critical impact parameter, $\sigma_A = \pi b_c^2$.

Many years ago, Darwin [19] derived an approximation for the deflection of null (massless) rays that pass close to the critical orbit. He found that the deflection angle is related to the impact parameter b by the equation

$$b - b_c = 216 \frac{3}{2}\sqrt{3}M \frac{\left(\frac{b}{3\sqrt{3}M} - 1\right)^{1/2}}{\left(\frac{b}{3\sqrt{3}M} + 1\right)^{1/2}} e^{-e} \approx 3.48M e^{-e} : \quad (5)$$

Using the same techniques, an approximation for the deflection of timelike (massive) geodesics can be derived. This calculation is outlined in Appendix A, and the result is

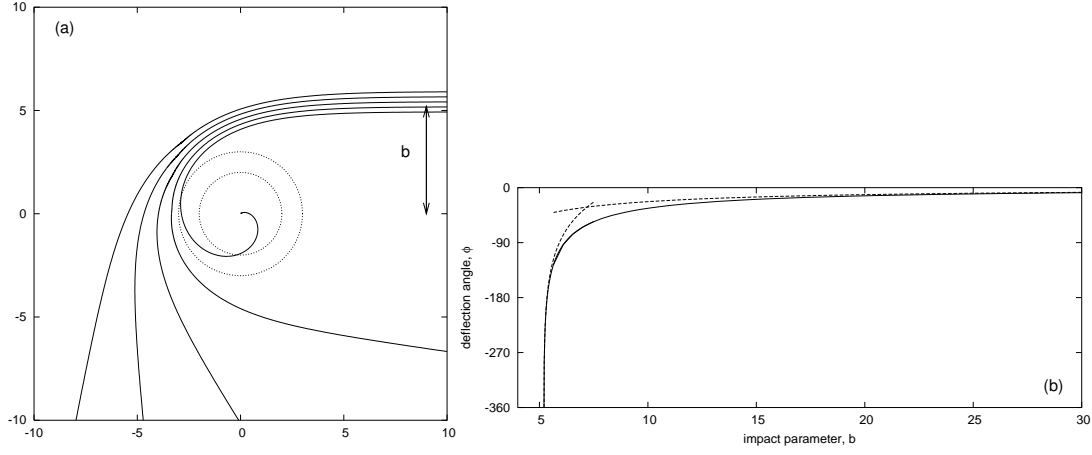


FIG. 1: (a) Photon geodesics around a Schwarzschild black hole, $M = 1$, close to the critical impact parameter $b_c = 3^{3/2} M \approx 5.196M$. The inner circle shows the event horizon at $r = 2M$, and the outer circle shows the unstable photon orbit at $r = 3M$. (b) Deflection angle as a function of impact parameter b . The plot compares the scattering angle with (i) the Einstein deflection angle $4M/b$, valid when $b > b_c$, and (ii) Darwin's approximation, $b = 3^{3/2} M + 3.48M e^{-b/b_c}$, valid when $b > b_c$.

$$b_c = M \frac{2^{13/2} e_c^3 (e_c + 3)^{3/2}}{v (e_c + 1)^{5/2}} \frac{1}{1 + \frac{1}{v} \frac{(e_c - 1)^{1/2}}{(e_c + 1)^{1/2}}} \exp \left(-\frac{r_c}{e_c + 3} \right) \exp \left(-\frac{r_c}{e_c + 3} \right); \quad (6)$$

where $e_c = (1 + 8v^2)^{1/2}$. This result reduces to equation (5) in the case $v = 1$.

A classical scattering cross section may be derived by considering a stream of parallel incident geodesics, as shown by Collins, Delbourgo and Williams [20]. Geodesics passing close to the critical orbit are scattered through angles that may be many multiples of 2π , so the total cross section is an infinite sum,

$$\frac{d\sigma}{d\Omega} = \frac{1}{\sin^2 \theta} \sum_{n=0}^{\infty} b_n(\theta) \frac{db_n}{d\theta}; \quad (7)$$

where the sum is taken over angles $\theta; 2\pi; 2\pi + \theta; 4\pi$, etc. The cross section is divergent in the forward direction, $d\sigma/d\Omega \approx 4v^4 (1 + v^2)^2 M^2 \theta^{-4}$ [20], due to the long-range nature of the interaction. It is also divergent (but integrable) in the backward direction, $d\sigma/d\Omega \approx 1/\theta^2$, because the element of solid angle tends to zero on-axis. The behaviour of the cross section close to $\theta = 0$ and $\theta = \pi$ may be understood using the approximations (3)

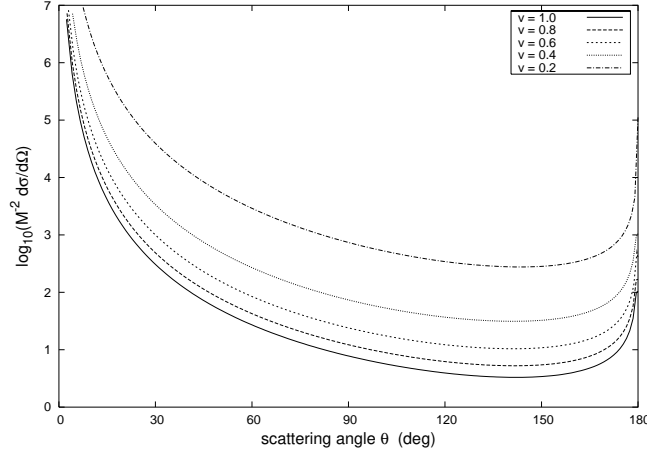


FIG. 2: Classical scattering cross sections for a range of particle speeds. The cross sections diverge on-axis at $\theta = 0$ and $\theta = 180^\circ$ as $\frac{d\sigma}{d\Omega} \sim 4v^4 (1 + v^2)^2 M^2 \theta^{-4}$ and $\frac{d\sigma}{d\Omega} \sim \frac{1}{\theta^2}$ respectively.

and (6) given above, and at intermediate angles it may be found by numerically integrating the elliptic equations. The result is plotted in Fig. 2 for a range of particle speeds.

B. Spin Precession

In the next section (III) we derive a semi-classical approximation to the massive fermion scattering cross section in the backward direction. To do this, we must first consider how the spin of the particle is affected by the gravitational interaction. For a massless wave, this is straightforward, as the helicity of the Dirac spinor remains unchanged. For a massive wave, the situation is substantially more complicated. However, progress can be made by considering the precession of the classical spin vector. We can then apply a semi-classical argument to relate the classical spin vector to the Dirac spinor itself in the r_s limit.

We begin by introducing an angular momentum four-vector s with components $[s^t; s^r; s^\theta; s^\phi]$, where $t; r; \theta; \phi$ are the coordinates of the standard Schwarzschild metric g . The four-vector s is spacelike, normalised, and orthogonal to the velocity v . Classically, angular momentum is parallel-transported along the geodesic, that is, $\underline{s} + v s = 0$. Inserting the standard Schwarzschild connection coefficients, and applying the orthogonality condition, we find the precession equations can be written as a pair of coupled first order

equations

$$\frac{ds}{d} + s^r = 0; \quad \frac{ds^r}{d} - (1 - \frac{3M}{r})s = 0; \quad (8)$$

where $s = rs$. Alternatively they can be combined in a simple second-order equation

$$\frac{d^2 s}{d^2} + \left(1 - \frac{3M}{r}\right)s = 0; \quad (9)$$

Now let us investigate a specific case, in which the spin vector is initially aligned with the direction of motion. At infinity, where $u = 0$, we start with initial conditions $s^r = 1$ and $s = 0$, where $\frac{d}{d} = (1 - \frac{3M}{r})^{1/2}$. The solutions to the precession equations may then be written as

$$\begin{aligned} s(u) &= \frac{1}{1 + u^2} \sin(u) \\ s^r(u) &= \frac{1}{1 + u^2} \cos(u) \\ (u=2) \frac{1}{1 + u^2} &= \frac{1}{2} \left(2Mu^3 - u^2 + 2M^2u + 1 \right)^{1/2} \sin(u); \end{aligned} \quad (10)$$

where $u = (bv)^{1/2}$ and

$$(u) = \int_0^u \frac{dw}{1 + w^2} - \frac{2M}{u^3} \left(w^2 + 2M^2w + 1 \right)^{1/2} dw; \quad (11)$$

For comparison, the scattering angle can be written in similar form as

$$(u) = \int_0^u \frac{dw}{2Mw^3 - w^2 + 2M^2w + 1} - \frac{1}{u^2} dw; \quad (12)$$

Equations (11) and (12) can be expressed in terms of elliptic functions, but we prefer to solve them numerically here.

In the next section we discuss glory scattering, which is related to the classical orbits that emerge in the backwards direction. We are particularly interested in the angle that the classical spin vector makes with the outgoing radial direction, in the rest frame of the particle. For a clockwise orbit, we define

$$\lim_{r \rightarrow 1} \tan^{-1} \frac{s}{s^r} = 2\theta_1; \quad (13)$$

where $\theta_1 = \theta(u_0)$, and $u_0 = 1/r_0$ is found from the radius of closest approach for the 180° orbit. The vectors and angles in Eq. (13) are illustrated in Fig. 3(a). Figure 3(b) plots for the backward-scattering orbit as a function of particle velocity, and demonstrates that decreases monotonically as v increases, from $\theta_1 = \pi/2$ at $v = 0$, to $\theta_1 = 0$ at $v = 1$.

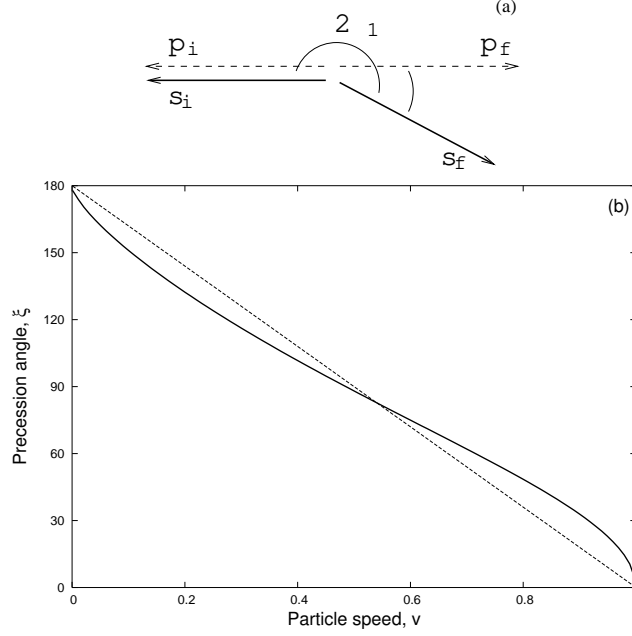


FIG. 3: Spin precession around a 180° orbit. (a) Depicting the precession angle ξ . Here, p_i and p_f are the initial and final momentum directions, and s_i and s_f are the initial and final spin directions in the rest frame of the particle. (b) The precession angle ξ (solid line) as a function of particle velocity v . The dotted line is for reference only.

III. SPINOR SCATTERING: ANALYTIC RESULTS

In this section we review some approaches to calculating the fermionic cross sections for black hole scattering. The appropriate method depends on the ratio of the black hole size to particle wavelength. A convenient dimensionless measure of the gravitational coupling is

$$\frac{GM_E}{\hbar c^3} = \frac{r_s}{\lambda} \quad (14)$$

where r_s is the Schwarzschild radius, and $\lambda = \hbar/p$ is the wavelength of the quantum particle. Reverting to natural units, we see that $\lambda = M_E$, which we use to label our figures.

A. Low-coupling scattering cross sections: Perturbation theory

In a recent paper [14], Doran and Lasenby showed that the fermion scattering cross section can be expanded as a perturbation series. In effect, they calculated the gravitational

analogue of the Mott formula for scattering from a Coulomb potential. The series takes the form

$$\frac{d}{d} = \frac{GM}{c^2} a_0(v; \theta) + a_1(v; \theta) + a_2(v; \theta) + \dots; \quad (15)$$

with a_i as defined above, and $a_i(v; \theta)$ dimensionless functions. The perturbation series approach is most appropriate in the long-wavelength limit, when $r_s \gg 1$. Doran and Lasenby showed that the first-order term a_0 is gauge-invariant and equal to

$$a_0(v; \theta) = \frac{1 + 2v^2 - 3v^2 \sin^2(\theta/2) + v^4 - v^4 \sin^2(\theta/2)}{4v^4 \sin^4(\theta/2)}; \quad (16)$$

In the massless limit ($v \rightarrow 1$), this reduces to the unpolarized Mott scattering formula. The cross section will tend to the first-order result (16) in the long wavelength limit, as $r_s \rightarrow \infty$. In Appendix B we show how to calculate the next term in the perturbation series in the Kerr-Schild gauge. We find

$$a_1(v; \theta) = -\frac{(3 + 4v^2 + v^4)(2 - j \sin(\theta/2)) - (7v + v^4) \sin^2(\theta/2)}{4v^3 j \sin(\theta/2)}; \quad (17)$$

The equivalent result for Coulomb scattering was successfully calculated by Dalitz [21] many years ago. The second order matrix element also allows the calculation of the degree of polarization P induced in an initially unpolarized beam. The net polarization is in the direction orthogonal to the plane of scattering, $p_i = p_f$. To first order,

$$P = \frac{GM}{c} \frac{v(3 + v^2) \tan^2(\theta/2) \ln(\sin^2(\theta/2))}{2(1 + 2v^2 - 3v^2 \sin^2(\theta/2) + v^4 - v^4 \sin^2(\theta/2))} \sin \theta \quad (18)$$

where we have included the dimensional constants for clarity. The confirmation of the gauge-invariance of results (17) and (18) awaits further work. In section V we compare the perturbation series and polarization with numerical results.

B. Higher-coupling scattering cross sections: Glory and spiral scattering

Many authors [8, 10, 11] have noted that black hole wave scattering produces diffraction effects that are familiar from optical phenomena. Two such effects are glory and spiral scattering. A glory is a bright spot or halo that appears on-axis in the backward direction from the scatterer. Spiral scattering, or orbiting, creates oscillations in scattered intensity at intermediate scattering angles. In a general analysis of semi-classical scattering, Ford and Wheeler [22] showed that both effects may be understood with reference to the deflection of

classical paths. A glory occurs whenever the deflection angle passes through a multiple of π , and spiral scattering occurs when paths orbit the scattering centre multiple times. For a discussion of the application of semi-classical techniques to the black hole case, see [11] or [16].

Ford and Wheeler [22] derived a semi-classical approximation of the glory scattering cross section for scalar ($s = 0$) waves. This approximation was extended to arbitrary spins by Zhang and DeWitt-Morette in [9] using path integral methods. For massless waves, the backward glory cross section is approximated by

$$\frac{d}{d\theta}_{\text{glory}} \approx 2 E b_g^2 \frac{db_g}{d\theta} = J_{2s}^2(E b_g \sin \theta); \quad (19)$$

where s is the spin of the particle, J_{2s} is a Bessel function, and b_g is the impact parameter at which $\theta = \pi$. In combination with Darwin's result (5) for the deflection of a massless particle that passes close to the horizon, we have $b_g = 5.3465M$, and $db_g/d\theta = 0.1504M$, so

$$M^2 \frac{d}{d\theta}_{\text{glory}} \approx 2 E M^2 4.30 J_{2s}^2(5.3465 E M \sin \theta); \quad (20)$$

For the scalar wave, the intensity has a peak in the backwards direction, whereas for the spinor wave the intensity is zero on-axis.

We now derive a similar approximation for the massive spin-half case, by taking into account the effects of classical spin precession. Let us begin by considering a backward-scattering orbit defined by $p_i = \hat{z} = p_f$, that lies in the z plane. As we saw in Section IIB, the classical spin vector is rotated by an angle of $2\alpha_1$ around this orbit. The quantum spin vector, on the other hand, is found by the double-sided action of the Dirac spinor, $s = \hbar \hat{j}^\alpha \hat{j}_\alpha$, where \hat{e}_α are the standard Dirac-Pauli matrices. Assuming that the classical and quantum spin vectors coincide in the classical limit, $\hbar \rightarrow 0$, we conclude that, in the rest frame, the Dirac spinor must transform according to

$$f / i = \cos(\alpha_1) \hat{1} + \sin(\alpha_1) \hat{e}_3 \quad (21)$$

where $\hat{1}$ is the identity matrix, and $\hat{e}_\alpha = \sin \alpha \hat{e}_1 + \cos \alpha \hat{e}_2$. Now consider the cross section on-axis. Following the arguments of Zhang and DeWitt-Morette [9], we note that there is a circular degeneracy here, and that paths from all scattering planes will interfere coherently. Around the circle $0 < \alpha < 2\pi$, the \hat{e}_3 term of (21) sums to zero, and the intensity on-axis is therefore proportional to $\cos^2(\alpha_1)$. Since it is the spinors, rather than the vectors, that are

summed coherently, the half-angle of precession arises naturally. The arguments of Zhang and DeWitt-Morette can be extended in a straightforward way to derive an approximation for angles close to $\pi/2$, leading to

$$\frac{d}{d\theta} \left(\frac{b}{b_0} \right) = \frac{2}{\cos^2(\theta/2)} J_0^2(E b \sin \theta/2) + \frac{2}{\sin^2(\theta/2)} J_1^2(E b \sin \theta/2); \quad (22)$$

Finally, we may use (6) to evaluate b at $\theta = \pi/2$, and substitute into the above result. Alternatively, we may choose to evaluate b_0 numerically for a more accurate result. In section V we compare both approaches with our numerical results.

IV. SPINOR WAVE SCATTERING

Before considering the Dirac equation on a Schwarzschild black hole background, we first discuss the general theory of relativistic spin-half scattering from a spherically-symmetric source.

A. Scattering from a spherically-symmetric source

In considering spherically-symmetric scattering we will employ the two-component spherical spinors that are eigenvectors of the angular equation

$$(\hat{L} + 1) \chi = 0; \quad (23)$$

where $\hat{L} = [\hat{L}_x; \hat{L}_y; \hat{L}_z]$ is the angular momentum operator, and the components of $\chi = [\chi_x; \chi_y; \chi_z]$ are Pauli spin matrices. Angular states are labelled by the eigenvalue j which is related to the overall angular momentum j by

$$j = \begin{cases} l + 1/2 & \text{where } l = j - 1/2 \\ l & \text{where } l = j \end{cases}; \quad (24)$$

Note that our sign convention for j may differ from the literature [23]. Explicitly, the spherical spinors are

$$\chi(j, m) = \sum_{m'=-l}^l C(l, m, m') Y_l^{m'}(\theta, \phi); \quad (25)$$

where $S = \frac{1}{2} \sigma_j$, $C(j_1 j_2 j_{\text{tot}}; m_1 m_2)$ are the Clebsch-Gordan coefficients, $Y_l^m(\theta; \phi)$ are spherical harmonics, and χ_{\pm}^m are the spin-up and spin-down spinors, $\chi_{\pm}^{\frac{1}{2}} = \begin{bmatrix} 1 \\ 0 \end{bmatrix}$ and $\chi_{\pm}^{-\frac{1}{2}} = \begin{bmatrix} 0 \\ 1 \end{bmatrix}$. The positive and negative spinors are related by

$$\chi_{\pm}^m = i \sigma_y \chi_{\pm}^{-m}; \quad (26)$$

where $\mathbf{r} = r^{-1} P_i \mathbf{x}^i$.

Consider, first, the free-particle Dirac equation, $\hat{H} \psi = 0$. It admits plane wave solutions; for example, a plane wave propagating in the z direction can be written as

$$\psi_{\text{plane}} = \begin{pmatrix} 0 \\ 1 \end{pmatrix} A e^{ipz} e^{iEt}; \quad (27)$$

It also admits separable solutions in spherical coordinates of the form

$$\psi = \frac{1}{r} \begin{pmatrix} u_1(r) \\ u_2(r) \end{pmatrix} A e^{iEt}; \quad (28)$$

where $u_1(r)$ and $u_2(r)$ are radial functions, and $\begin{pmatrix} 0 \\ 1 \end{pmatrix}$ the Pauli two-component spherical spinors (25). The free particle radial equations can be written in matrix form as

$$\frac{d}{dr} \begin{pmatrix} u_1 \\ u_2 \end{pmatrix} = \begin{pmatrix} 0 & 1 \\ -i(E-m) & 0 \end{pmatrix} \begin{pmatrix} u_1 \\ u_2 \end{pmatrix}; \quad (29)$$

and their solutions are spherical Bessel functions

$$u_1^{(\pm)}(r) = r j_l(pr); \quad u_2^{(\pm)}(r) = \frac{ipS}{E+m} r j_l(pr); \quad (30)$$

where $l = l + S$. The plane wave solution (27) can be written as a sum of spherical solutions (28), as

$$\psi_{\text{plane}}^{(\pm)} = e^{iEt} \sum_{l=0}^{\infty} \frac{1}{r} \begin{pmatrix} u_1^{(\pm)} \\ u_2^{(\pm)} \end{pmatrix} A; \quad (31)$$

The asymptotic behaviour of the radial solutions is found by noting

$$j_l(pr) \sim \frac{1}{pr} \sin pr - \frac{1}{2}; \quad \text{as } r \rightarrow \infty; \quad (32)$$

When an interaction is introduced, the unperturbed plane wave is no longer an eigenstate of the Hamiltonian. Instead we look for a time-independent solution with the asymptotic behaviour

$$\psi \sim \psi_{\text{plane}} + \frac{C}{r} e^{ipr} e^{iEt}; \quad (33)$$

where C is a four-component spinor to be determined. Asymptotically, the wave function is interpreted as the sum of an incident plane wave and a radially-outgoing scattered wave. The effect of an interaction is to introduce phase shifts into the asymptotic solution (32). We define an interaction phase shift by comparing the asymptotic solution with the free-space form (32),

$$u_1^{(+)}(r) \sim p^{-1/2} \sin(pr - \frac{1}{2}\pi + \delta_l); \text{ as } r \rightarrow \infty; \quad (34)$$

An expansion of the form (33) is only strictly valid if the interaction is localised. In a long-range potential, such as the Coulomb $1/r$ potential, the asymptotic solutions are modified by the presence of a radially-dependent phase factor. The same is true in a gravitational field, as we show in the next section. The extra phase factor means that incident plane waves are distorted by the presence of the potential even at infinity. However, the extra phase shift is independent of l , so does not contribute to δ_l and the phase difference between partial waves.

Let us now assume that the wave is incident along the z -axis, and is in a superposition of spin-up and spin-down states, with upper components

$$\sum_{m=-\frac{1}{2}}^{\frac{1}{2}} C_m u_m = \begin{pmatrix} C_{\frac{1}{2}} \\ C_{-\frac{1}{2}} \end{pmatrix} A; \quad (35)$$

We now construct a partial wave series with asymptotic form (33). For clarity we need only consider the upper components of the scattered wave, given by

$$\text{Upper}(C) = \sum_m C_m B_m; \quad (36)$$

where

$$B_m = \frac{(4\pi)^{1/2}}{2ip} (2l+1)^{1/2} (e^{2i\delta_l} - 1) C(l, \frac{1}{2}; 0, m) C(l, \frac{1}{2}; m, \frac{1}{2}) / C(l, \frac{1}{2}; 0, \frac{1}{2}) C(l, \frac{1}{2}; \frac{1}{2}, 0); \quad (37)$$

Using the properties of Clebsch-Gordan coefficients, it is straightforward to show that $B_{1/2}^{1/2} = B_{-1/2}^{-1/2}$. The scattered wave spinor can be written as $A \begin{pmatrix} B_{1/2}^{1/2} \\ B_{-1/2}^{-1/2} \end{pmatrix}$, where A is a transition amplitude matrix, with components

$$A = \begin{pmatrix} B_{1/2}^{1/2} & B_{-1/2}^{-1/2} \\ B_{1/2}^{-1/2} & B_{-1/2}^{1/2} \end{pmatrix} A = f(\theta) + ig(\theta) \hat{n}; \quad (38)$$

Here, f and g are complex amplitudes, and it can be shown (see, for example, [23]) that the rotation vector \hat{n} is orthogonal to both the incident and scattered direction, $\hat{n} = \mathbf{p}_i \times \mathbf{p}_f = \mathbf{p}_i \times \mathbf{p}_s$. The scattered intensity from an unpolarized beam is the sum of the squares of the amplitudes,

$$\frac{d}{d\Omega} = |f|^2 + |g|^2 \quad (39)$$

In terms of phase shifts, the scattering amplitudes are

$$f(\theta) = \frac{1}{2ip} \sum_{l=0}^{\infty} (l+1) (e^{2i\delta_{l+1}} - 1) + l(e^{2i\delta_l} - 1) P_l(x) \quad (40)$$

$$g(\theta) = \frac{1}{2ip} \sum_{l=0}^{\infty} (e^{2i\delta_{l+1}} - e^{2i\delta_l}) P_{l+1}^1(x) \quad (41)$$

where $x = \cos \theta$. There are two limiting cases to consider. First, in the non-relativistic limit we expect the interaction to depend only on orbital angular momentum (l). In this case, we expect $\delta_{l+1} = \delta_l$, and the spin is then unchanged by the interaction, and we recover the non-relativistic scattering series $(2ip)^{-1} \sum_{l=0}^{\infty} (2l+1) e^{2i\delta_l} P_l(x)$ (where $\delta_l = \delta_{l+1} = \delta_{l-1}$).

Second, in the highly-relativistic regime $E \gg m$, the phase shifts instead depend only on total angular momentum (j), and so $\delta_l = \delta_{l+1}$. Then, for $\theta \neq 0$,

$$f(\theta) = \frac{1}{2ip} \sum_{l=0}^{\infty} (l+1) e^{2i\delta_{l+1}} [P_{l+1}(x) + P_l(x)] \quad (42)$$

$$g(\theta) = \frac{1}{2ip} \sum_{l=0}^{\infty} e^{2i\delta_{l+1}} [P_{l+1}^1(x) - P_l^1(x)] \quad (43)$$

Using the properties of the Legendre polynomials, it is straightforward to show (eg. Mott [24]) that

$$g = \tan(\theta/2) f \quad (44)$$

in the relativistic limit. Physically, this implies that the helicity of a massless wave remains unchanged by the interaction.

If the particle has mass then the scattered beam may become partially polarized by the interaction. The degree of polarization P induced in an initially unpolarized beam is

$$P = \frac{|f|^2 - |g|^2}{|f|^2 + |g|^2} \quad (45)$$

in the direction \hat{n} . This effect is known as Mott polarization, and is well known for the Coulomb interaction of an electron with a nucleus. Conversely, if the incident beam is already partially polarized (with polarization vector \mathbf{P}) then the wave is scattered asymmetrically, with asymmetry factor $P \cdot \hat{n}$.

B. The Dirac equation on a Schwarzschild background

We now consider the Dirac equation on a Schwarzschild spacetime. Before starting, we must choose an appropriate coordinate system. A disadvantage of standard Schwarzschild coordinates is that they are valid only in the exterior region, $r > 2M$. Geodesics do not cross the horizon in a finite Schwarzschild coordinate time, and all solutions to the wave equation are singular at the horizon. Here, we prefer to work with coordinate systems that remove the coordinate singularity at $r = 2M$. Two possibilities are advanced Eddington-Finkelstein coordinates, with metric

$$ds^2 = (1 - 2M/r)dt^2 - (4M/r)dt dr - (1 + 2M/r)dr^2 - r^2 d\Omega^2; \quad (46)$$

and Painlevé-Gullstrand coordinates [14, 25], with metric

$$ds^2 = (1 - 2M/r) dt^2 - \sqrt{2M/r} dt dr - dr^2 - r^2 d\Omega^2; \quad (47)$$

Both coordinate systems deal smoothly with the horizon, and cover regions I and III of the Penrose diagram of the fully extended Kruskal manifold [26]. For a discussion of gauge-invariance and the choice of coordinates, see [27].

The time coordinate of the Painlevé-Gullstrand (PG) system has a simple physical interpretation. It corresponds to the proper time as measured by a observer in freefall who starts from rest at infinity. For this reason, we now formulate the Dirac equation on a black hole background described by PG coordinates.

We let $\sigma_0; \sigma_1; \sigma_2; \sigma_3$ denote the gamma matrices in the Dirac-Pauli representation, and introduce spherical polar coordinates $(r; \theta; \phi)$. From these we define the unit polar matrices

$$\begin{aligned} \sigma_r &= \sin \theta (\cos \phi \sigma_1 + \sin \phi \sigma_2) + \cos \theta \sigma_3; \\ \sigma_\theta &= \cos \theta (\cos \phi \sigma_1 + \sin \phi \sigma_2) - \sin \theta \sigma_3; \\ \sigma_\phi &= -\sin \theta \sigma_1 + \cos \theta \sigma_2; \end{aligned} \quad (48)$$

In terms of these we define four position-dependent matrices $g_t; g_r; g_\theta; g_\phi$ by

$$\begin{aligned} g_t &= \sigma_0 + \frac{r}{2M} \sigma_r; & g_r &= \sigma_r; \\ g_\theta &= \sigma_\theta; & g_\phi &= \sigma_\phi. \end{aligned} \quad (49)$$

These satisfy the anti-commutation relations

$$fg_{\pm}g_{\pm} = 2g_{\pm}I \quad (50)$$

where g_{\pm} is the Painlevé-Gullstrand metric of equation (47). The reciprocal matrices $g^t; g^r; g_{\pm}$ are defined by the equation

$$fg_{\pm}g_{\pm} = 2I; \quad (51)$$

and both sets are well-defined everywhere except at the origin.

The Dirac equation for a spin-half particle of mass m is

$$ig \not{r} = m; \quad (52)$$

where

$$\not{r} = (\not{\partial} + \frac{i}{2} \not{\partial} \not{r}) ; \quad \not{\partial} = \frac{i}{4} [\not{\partial} ; \not{r}] ; \quad (53)$$

The components of the spin connection are found in the standard way [28] and are particularly simple in the Painlevé-Gullstrand gauge [27],

$$g \frac{i}{2} \not{\partial} \not{r} = \frac{3}{4r} \frac{2M}{r} \not{\partial} ; \quad (54)$$

An advantage of our choice of metric is that the Dirac equation can now be written in a manifestly Hamiltonian form

$$i\partial_t + i^0 \frac{2M}{r} \not{\partial} \not{r} = m; \quad (55)$$

where $\not{\partial}$ is the Dirac operator in flat Minkowski spacetime. The interaction term is non-Hermitian, as the singularity acts as a sink for probability density, making absorption possible.

The Dirac equation is separable in time, with solutions that go as $\exp(-iEt)$. The energy E conjugate to time-translation is independent of the chosen coordinate system, and has a physical definition in terms of the Killing time [27]. We exploit the spherical symmetry to separate the spinor into

$$= \frac{e^{-iEt}}{r} \begin{pmatrix} u_1(r) \\ u_2(r) \end{pmatrix} \begin{pmatrix} 0 \\ 1 \end{pmatrix}_A \quad (56)$$

The trial function (56) results in a pair of coupled first-order equations

$$(1) \quad \frac{d}{dr} \left(\frac{0}{2M=r} \right) \frac{1}{u_2} = \frac{0}{2M=r} \frac{1}{u_2} + \frac{1}{2M=r} \frac{1}{u_2} \quad (57)$$

$$\begin{aligned}
U_1^{(\text{out})} &= e^{i p r} e^{i(\alpha_1 + \alpha_2)} \mathcal{A} \begin{matrix} 0 & 1 \\ 1 & A \\ p=(E+m) & 1 \\ 0 & 1 \end{matrix} \\
U_1^{(\text{in})} &= e^{-i p r} e^{i(\alpha_1 - \alpha_2)} \mathcal{A} \begin{matrix} 1 & A \\ p=(E+m) \end{matrix} \quad (61)
\end{aligned}$$

where the phase factors $\phi_1(\mathbf{r}); \phi_2(\mathbf{r})$ are given by

The general solution as $r \rightarrow 1$ is a superposition of the ingoing and outgoing waves,

for each angular mode. The magnitudes of A^{in} and A^{out} determine the amount of scattered and absorbed radiation present. The phase shift is given by their ratio,

D . Numerical Method

18

that they are sufficiently close to the boundary points. The phase shift should also be independent of the choice of coordinates. We repeated our analysis using Eddington-Finkelstein coordinates to check the numerical accuracy of our results.

For the scalar wave in the large- l limit [16] the phase shifts approach "Newtonian" values which arise in a strict $1/r$ potential,

$$e^{2i\delta_l^N} = \frac{(1 + \frac{1}{2} - i)}{(1 + \frac{1}{2} + i)}; \quad (65)$$

where $\frac{1}{2} = M(2E^2 - m^2)/p = M/E(1 + v^2) = v$. Phase shifts of this form also occur in the non-relativistic Coulomb scattering problem (see, for instance, [24]), with $\frac{1}{2} = Zm/p$. It is well known that the problem of non-relativistic Coulomb scattering can be solved exactly in parabolic coordinates (see, for example, [33]). The pure-Newtonian phase shift series defined by

$$f_N(\theta) = \frac{1}{2ip} \sum_{l=0}^{\infty} (2l+1) \frac{(1 + \frac{1}{2} - i)}{(1 + \frac{1}{2} + i)} P_l(\cos \theta) \quad (66)$$

can be summed using the Coulomb result to

$$f_N(\theta) = \frac{(1 - i)}{2p(1 + i)} [\sin(\theta/2)]^{2+2i} : \quad (67)$$

It is more difficult to sum the series (66) directly, because it is poorly convergent. This is related to the fact that an infinite number of Legendre polynomials are required to describe the divergence at $\theta = 0$. Many years ago, Yennie, Ravenhall and Wilson [34] outlined one possible way around this problem. Given a Legendre polynomial series

$$f(\theta) = \sum_{l=0}^{\infty} a_l^{(0)} P_l(\cos \theta) \quad (68)$$

that is divergent at $\theta = 0$, one may define the m th reduced series,

$$(1 - \cos \theta)^m f(\theta) = \sum_{l=0}^{\infty} a_l^{(m)} P_l(\cos \theta) : \quad (69)$$

The reduced series is obviously less divergent at $\theta = 0$, so one may hope that the reduced series converges more quickly. Using the properties of the Legendre polynomials, it is straightforward to show that the new coefficients $a_l^{(i+1)}$ are related to the old coefficients $a_l^{(i)}$ by the iterative formula

$$a_l^{(i+1)} = a_l^{(i)} - \frac{1 + \frac{1}{2}}{2l + 3} a_{l+1}^{(i)} - \frac{1}{2l - 1} a_{l-1}^{(i)} : \quad (70)$$

We have found that this to be an excellent method for summing the series numerically, and that two or three iterations are sufficient.

V. NUMERICAL RESULTS

In this section we present the results of our numerical calculations, and compare with theoretical expectations outlined in sections II and III.

A. Absorption Cross Sections

The existence of an ingoing current at the horizon implies that flux is absorbed by the black hole. The absorption cross section σ_A is defined as ratio of the absorbed and incident fluxes. For the spin-half wave,

$$\sigma_A = \frac{X}{p^2} \sum_{j=0}^{\infty} |j-1| \left| \frac{f_j^{2i}}{f_j} \right|^2 : \quad (71)$$

At low energies, absorption is dominated by the $j = s$ mode. For massless waves, the low energy limits are: (i) $\sigma_A = 16 M^2$ for $s = 0$, (ii) $\sigma_A = 2 M^2$ for $s = 1=2$, (iii) $\sigma_A = \frac{64}{3} (M E)^2 M^2$ for $s = 1$, and (iv) $\sigma_A = \frac{256}{45} (M E)^4 M^2$ for $s = 2$ (see [35]). Note that the low-energy scalar and spinor cross sections are proportional to the black hole area, whereas the electromagnetic and gravitational cross sections tend to zero in this limit.

The massless scalar and fermion cross sections are shown in the left panel of Fig 4. For massive particles, the cross section diverges in the low energy limit, as shown in the right panel of Fig 4. In all cases, the cross section approaches the geometrical optics value of $\sigma_A = 27 M^2$ in the high-energy limit. For more details on the absorption cross sections of massive spin-half particles, see Doran et al. [36].

B. Scattering at low couplings, r_s

In section III we outlined our expectations for scattering at low couplings. We now test them numerically. Figure 5 compares the perturbation series (15) with a numerically-calculated cross section, at $M E = 0.04$ and $v = 0.6$. It is clear that the approximation is improved by the inclusion of the second-order term, Eq. (17).

Figure 6 compares the perturbation results with the numerical calculations across a range of values of $M E$ and v . The first-order series (16) is shown as a dotted line, and the second-order series (17) is shown as a dashed line. As expected, we find that the second-order correction improves the fit, and the approximation is in excellent agreement when

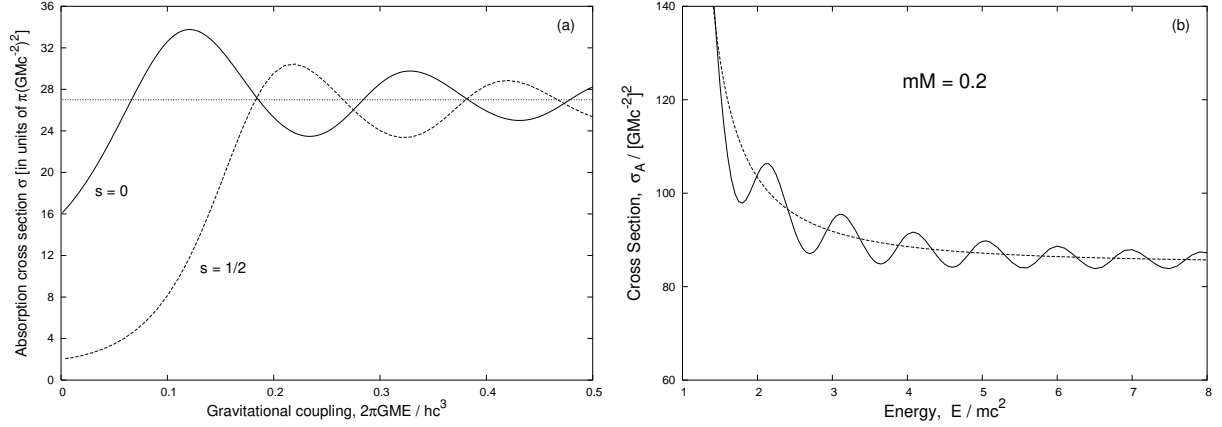


FIG. 4: Absorption cross section. (a) Massless. Shows the absorption cross section of a massless scalar [solid] and a massless fermion [dashed]. The classical limit at 27 is also marked. (b) Massive. The solid line shows the quantum absorption cross section for $GmM \approx c = 0.2$, and the dotted line is the classical cross section (4).

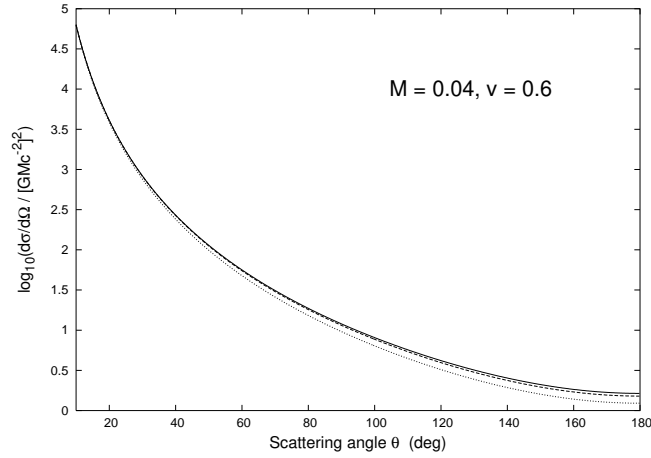


FIG. 5: Comparison of the numerical cross section [solid] with the first-order [dotted] and second-order [dashed] Born approximation at $ME = 0.04$, $v = 0.6$. Note that the scale on the y-axis of the left plot is logarithmic.

$MEv \approx 0.1$. At higher couplings, the truncated perturbation series is still accurate for small scattering angles, but it fails to predict glory and spiral scattering oscillations. In this regime, $r_s \approx 1$, a full numerical calculation is necessary.

The perturbation calculation also predicts the magnitude of Mott polarization, which we

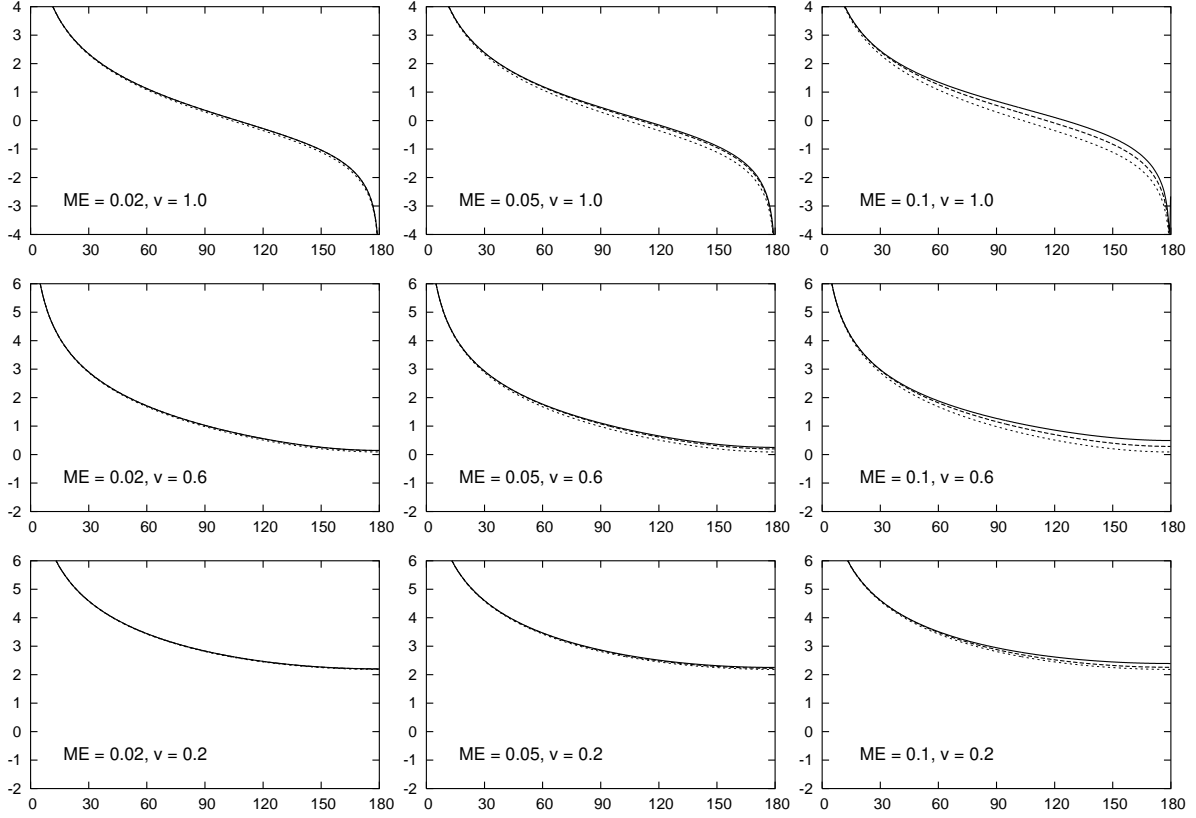


FIG. 6: Comparison of the numerical cross section [solid] with the first-order [dotted] and second-order [dashed] Born approximation across a range of ME and v . The x-axis shows the scattering angle (deg) and the y-axis shows the cross section, $\log_{10} M^{-2} \frac{d}{d\delta}$.

now test against numerical results. The first-order polarization is given by (18), whereas the numerical polarization is determined by (45). Figure 7 compares the perturbation series and numerical results for a low coupling, $ME = 0.002$. The left-hand plot (a) shows that there is an order-of-magnitude agreement between the two results. Naively, in the limit $ME \rightarrow 0$, we would expect to find perfect agreement between the two. We do not observe this. However, it is remarkable that we can obtain excellent agreement by artificially removing the effects of absorption from the numerical results. If we set the imaginary part of the numerical phase shifts to zero, we obtain the right-hand plot, Fig. 7 (b). It is apparent therefore that the perturbation method is somewhat flawed, as it does not account for absorptive effects. This is related to the fact that, whereas plane waves form a complete basis for the hydrogen atom, they do not form a complete basis on a black-hole spacetime. We discuss this problem

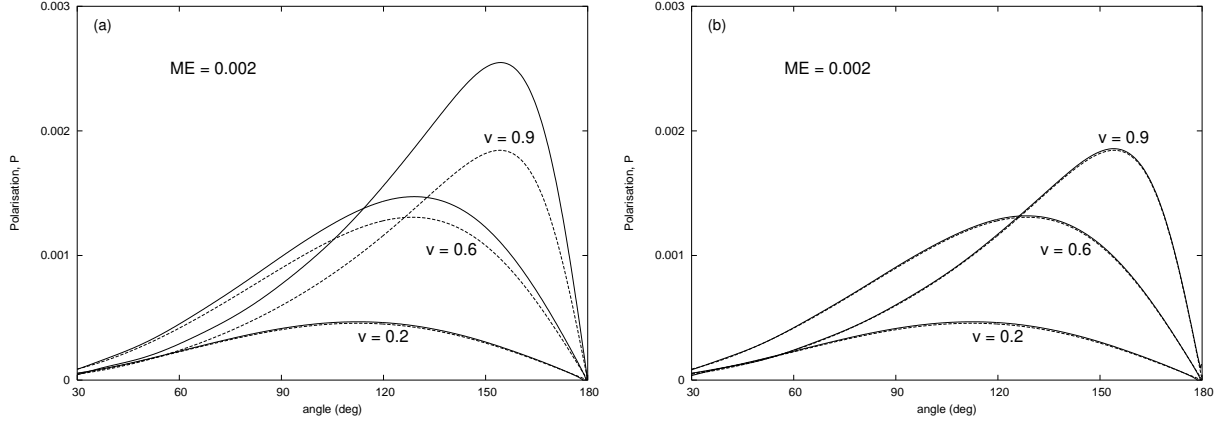


FIG. 7: Comparison of the numerical polarization [solid] and the perturbation calculation (18) [dotted] for $ME = 0.002$. (a) With absorption. The perturbation result (18) does not match the numerical result. (b) Without absorption. Enforcing the artificial condition that numerical phase shifts are purely real removes the effect of absorption (see text). We then observe an excellent agreement with the perturbation result.

further in Section VI.

C. Scattering at higher couplings, ϵ_2

Figure 8 shows numerically-determined scattering cross sections for a massless fermion at larger couplings. As expected, we observe spiral scattering oscillations, and a zero on-axis in the backward direction. The magnitude of the oscillations, and their angular frequency, increases with black hole mass. The zero in the backward direction can be verified by substituting $P_1(\theta) = (-1)$ into the partial wave series (42). The massless glory approximation (20) of Zhang and DeWitt-Morette [9] proves a good fit to the numerical results close to $\theta = 180^\circ$, as shown in Fig. 9. It correctly predicts the approximate magnitude and angular width of the oscillations.

The scattering cross sections for massless scalar and spinor waves are compared in Fig. 10. In the backward direction the scalar wave is at a maximum on-axis, whereas the spinor wave is at a minimum, as predicted by the glory approximation. At intermediate angles, the regular oscillations in the intensity of the scalar and spinor waves appear to be 180° out of phase.

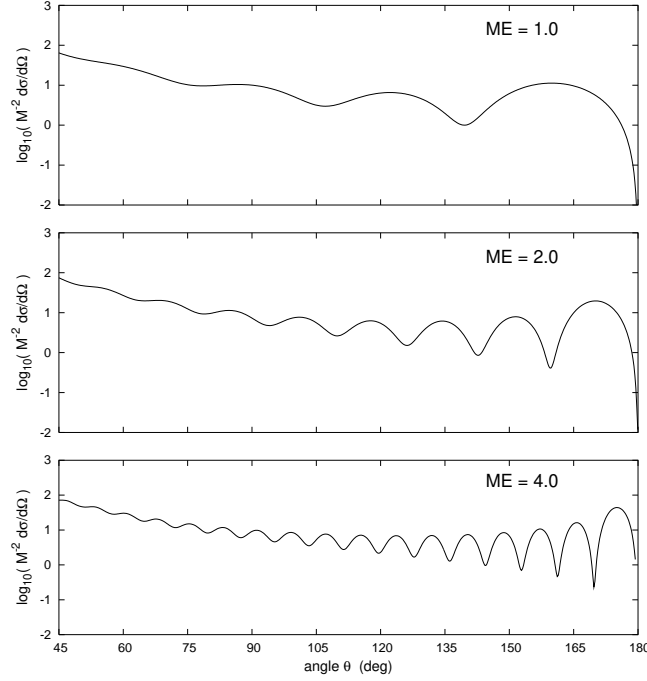


FIG. 8: Glory scattering cross sections for the massless spin-half wave for various couplings ME . $GM/E \sim c^3$.

Scattering cross sections for the massive spin-half wave are shown in Fig. 11. Here, the solid line shows the partial-wave result, and the broken lines show the semi-classical approximations to the glory (22). The dotted line is the result of using the modified Darwin approximation (6), and the dashed line is calculated by integrating the orbit equations numerically. It is clear that the numerical approach (dashed) provides the better fit. This is because, for slower particles, we find b_{glory} is too far from b_c for the first-order Darwin approximation to be sufficient. In general, the Darwin approximation underestimates the magnitude of the glory.

Figures 12 (a) and 12 (b) show the magnitude of Mott polarization as a function of scattering angle, for a range of couplings. The relationship between polarization, scattering angle, particle velocity, and black hole mass is not immediately obvious. However, Fig. 13 shows that the oscillations in polarization are clearly related to the glory and spiral scattering oscillations, suggesting a semi-classical model for Mott polarization may be possible. This awaits further work.

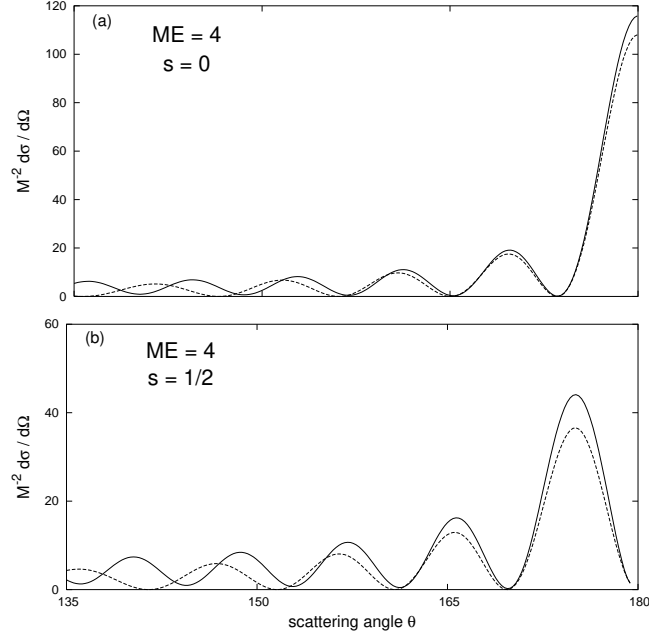


FIG . 9: Glory oscillations for the massless spinor and scalar waves. This plot compares the numerical glory oscillations (solid) with the approximate formula in the text (20) (dotted). (a) Scalar, $s = 0$. (b) Spinor, $s = 1/2$.

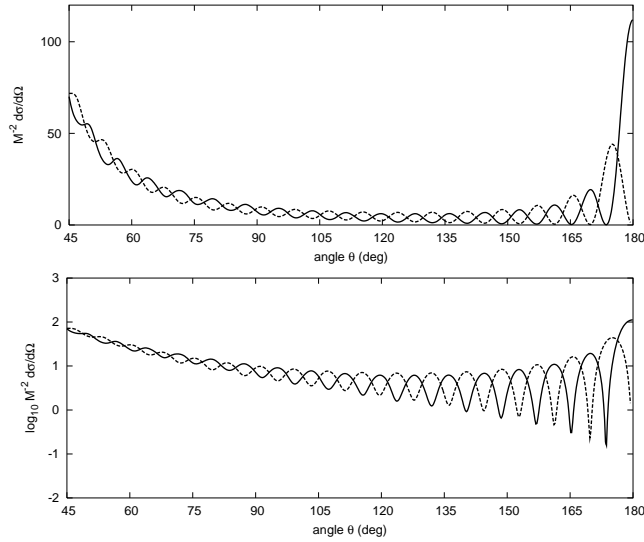


FIG . 10: Scattering cross sections for the massless scalar [solid] and spinor [dashed] waves at a coupling of $ME = 4$. Note that the bottom plot shows the same data as the top plot but with a logarithmic scale on the y-axis.

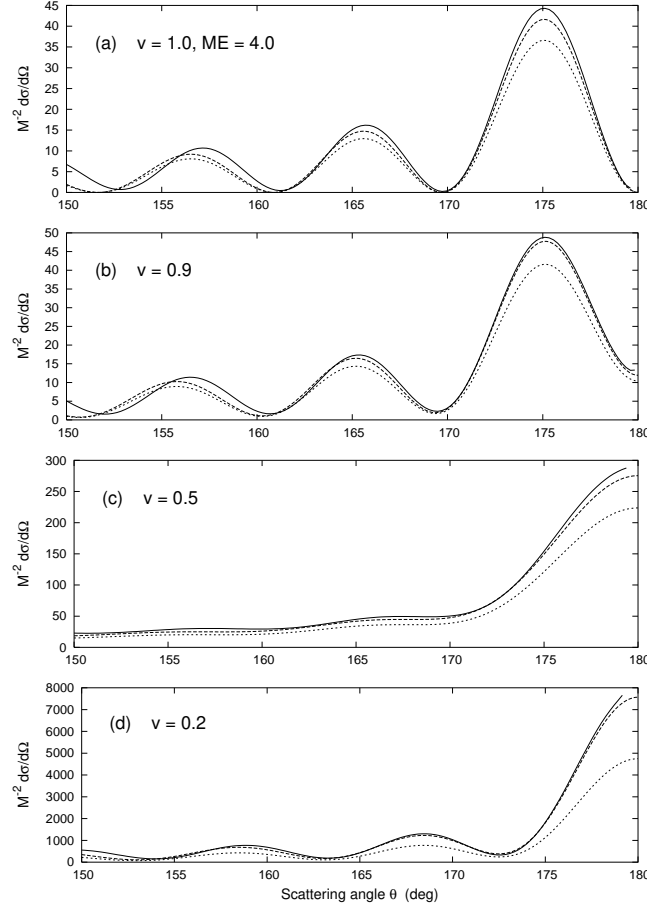


FIG. 11: Glory oscillations for the massive spin-half wave, over a range of particle speeds v . The solid line shows the numerical cross section. The dashed line shows the result of the semi-classical approximation (22), and the dotted line shows the result of using the modified Darwin approximation to estimate the glory impact parameter.

V I. D I S C U S S I O N A N D C O N C L U S I O N S

In this paper we have presented an investigation into the scattering and absorption of massive spin-half waves by a Schwarzschild black hole. We extended the approximations of Darwin [19] and Zhang and D eW itt-M orette [9] to derive a semi-classical (r_s) approximation for massive fermion glory scattering. We also took the perturbation analysis of D oran and L a s e n b y [14] to next order, to derive new formulae for the scattering cross section and Mott polarization in the low coupling limit, r_s . Finally, we applied partial-wave techniques to solve the D irac equation on the Schwarzschild spacetime, and presented our

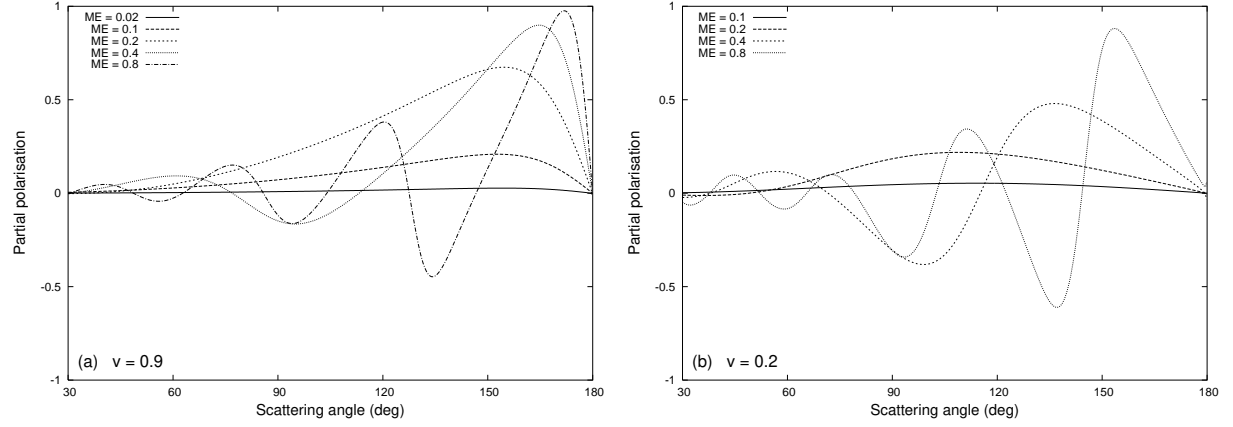


FIG. 12: Mott polarization as a function of scattering angle for a range of ME . Waves with mass are partially polarized by the interaction. As the coupling ME is increased, oscillations arise in the polarization. (a) For $v = 0.9$. (b) For $v = 0.2$.

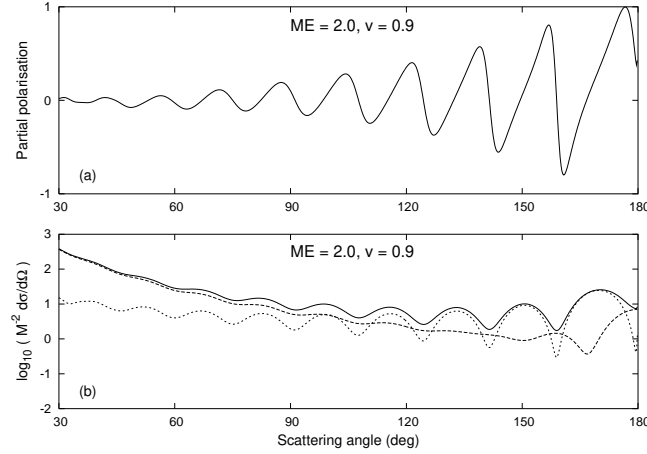


FIG. 13: Glory oscillations and polarization for $ME = 2$ and $v = 0.9$. (a) Partial polarization, P . (b) Scattering cross section. The solid line shows the total cross section, and the dotted and dashed lines show the contributions from the amplitudes f and g defined by Eq. (40) and (41).

numerical results. We showed that our approximations provide good fits to the numerical results in the appropriate limits.

We showed that non-zero particle mass leads to a phenomenon familiar from electromagnetic scattering: Mott polarization. This is a partial polarization created in the direction orthogonal to the scattering plane. In the electromagnetic case, an estimate of the polariza-

tion arises from the second-order term in the Born approximation [21]. In the gravitational case, a similar estimate arises from our second-order perturbation analysis in the Kerr-Schild gauge, Eq. (18). However, our estimate only agrees with the numerical calculation if we artificially suppress black hole absorption (see Fig. 7). This highlights a shortcoming in the Born approximation method: it cannot account for absorption effects. To see why, consider the Hamiltonian form of the Dirac equation in PG coordinates, Eq. (55). As $r \rightarrow 0$, all solutions go as $r^{3/4}$, and have a net ingoing current. Clearly, such solutions cannot be described by a linear sum of plane waves used in the Born approximation. A related observation is that the Hamiltonian is not Hermitian as probability flux is removed at the origin [27]. It is not immediately clear how we extend the Born approximation to such open systems. Despite such difficulties, however, we have seen that the Born approximation in its present form provides a good fit to numerical scattering cross sections when $r_s \ll r$, and it remains a useful tool.

One intriguing question raised by this work is: when, if ever, are fermion diffraction patterns from black holes of physical relevance? Since diffraction effects are only significant when $r_s \sim \lambda$, the question may be rephrased: do small black holes exist in nature? By small, we mean black holes with an event horizon smaller than the Compton wavelength of the lightest fermion (thought to be the electron neutrino). Recent experimental evidence suggests that neutrinos have non-zero mass. A neutrino with a hypothetical mass $m_\nu = 0.01$ eV has a Compton wavelength of 1.2×10^5 m, and this size corresponds to a black hole of mass $M = 10^{22}$ kg. Black holes of this magnitude or smaller are unlikely to be created by astrophysical processes; however, it is possible that small primordial black holes were created in the early universe. An alternative scenario for small black hole genesis arises in recently-proposed theories with Large Extra Dimensions [37]. If such theories are well-founded, it is possible that black holes may one day be created at a particle accelerator (see [38] for a review of these ideas).

Despite these possibilities, fermion diffraction patterns may never be observed. A more physically-relevant problem is that of gravitational-wave scattering from rotating, large black holes ($M > 10^{30}$ kg). Previous studies of massless spin-two waves on the Kerr spacetime have shown that the situation is complicated by effects including frame-dragging, spin-rotation coupling, and superradiance. Futterman, Handler and Matzner [16] present $s = 2$ scattering cross sections for a special case: the alignment of black hole spin axis and incident

wave momentum. However, we are not aware of a general analysis of o -axis gravitational scattering, though progress has been made for the simpler spin-zero case [39]. We suggest that a general study of spin-half scattering from a Kerr black hole would be a useful addition to the literature, for two reasons. Firstly, Unruh [40] has shown that superradiance does not occur for massless spin-half waves. Secondly, though we would expect to see the effects of spin-rotation coupling, the fewer degrees of freedom in the $s = 1/2$ case will make the results easier to interpret. Such a study would contribute to our understanding of gravitational-wave scattering, as well as being interesting in its own right. We therefore hope to extend the methods of this paper to the Kerr black hole in the near future.

APPENDIX A: NEAR-HORIZON SCATTERING APPROXIMATION

In [19], Darwin derived an approximation for the deflection of an unbound massless particle passing close to the horizon. Here we extend that calculation to the massive case, where $v < 1$.

Following the approach of Chandrasekhar [15], we look for roots of the orbit equation (2). For unbound orbits that avoid the singularity, the orbit equation has three real roots, $u_1 < 0, u_3 > u_2 > 0$. The roots can be written in terms of the eccentricity e and latus rectum l

$$u_1 = -\frac{e-1}{l}; \quad u_2 = \frac{e+1}{l}; \quad u_3 = \frac{1}{2M} - \frac{2}{l} \quad (\text{A } 1)$$

where e and l satisfy

$$\frac{1}{Ml} (3 + e^2) = \frac{1}{v^2 b^2};$$

$$\frac{1}{l^2} (e^2 - 1)(1 - 4) = \frac{1}{b^2}; \quad (\text{A } 2)$$

and $b = M = 1$. Making the substitution $u = (1 + e \cos \varphi) = l$ in (2) yields

$$\frac{d}{d\varphi} = (1 - 6 + 2e)^{1/2} - 1 - k^2 \cos^2(\varphi/2) \quad (\text{A } 3)$$

where

$$k^2 = \frac{4e}{1 - 6 + 2e} \quad (\text{A } 4)$$

The variable φ runs from 0 to $\varphi_1 = \cos^{-1}(e^{-1})$. The solutions of (A 3) are elliptic functions, and we can write the final angle as

$$\varphi_1 = \frac{2}{(1 - 6 + 2e)^{1/2}} K(k) - F\left(\frac{1}{2}, \frac{1}{2} - \varphi_1; k\right) \quad (\text{A } 5)$$

The critical orbit occurs where $u_2 = u_3$, $k = 1$. Then

$$\begin{aligned} e_c &= \sqrt{1 + 8v^2}; \\ l_c &= 2M \left(\sqrt{1 + 8v^2} + 3 \right); \\ b_c &= \frac{\sqrt{8v^4 + 20v^2} \sqrt{1 + (1 + 8v^2)^{3/2}} M}{2v^2}; \end{aligned} \quad (\text{A } 6)$$

The critical parameters are functions of the particle speed v only and lie in the ranges $1 \leq e_c \leq 3$, $8M \leq l_c \leq 12M$, and $3M \leq b_c \leq 4M$. We now consider orbits close to the critical orbit, by expanding in a power series in $\epsilon = 1 - l$

$$\begin{aligned} l &= l_c + \epsilon; \\ e &= e_c + \frac{4v^2}{(e_c + 1)(e_c + 3)M} \epsilon; \\ b &= b_c + M \frac{\sqrt{e_c}}{2\sqrt{2v(e_c + 3)^{1/2}}(e_c + 1)^{5/2}} \frac{\epsilon^2}{M^2}; \\ k^2 &= 1 - \frac{1}{e_c(e_c + 3)M} \epsilon; \end{aligned} \quad (\text{A } 7)$$

Note that b varies only quadratically with ϵ . We employ the following approximations for the elliptic functions

$$\begin{aligned} K(k) &\approx \ln \frac{4}{(1 - k^2)^{1/2}}; \\ F(z; 1) &\approx \frac{1}{2} \ln \frac{1 + \sin z}{1 - \sin z}; \end{aligned} \quad (\text{A } 8)$$

and substitute into (A 5). Finally, we define the deflection $\delta = 2 - \alpha$ to obtain result (6).

APPENDIX B: SECOND-ORDER BORN SERIES

Doran and Lasenby [14] showed how to calculate the first-order contribution to the fermion cross section in a consistent way. By expanding the scattering amplitude as a power series in the black hole mass M , they found the first term in the scattering amplitude series to be

$$M^{-1} \bar{u}_s(p_f) \hat{1} u_r(p_i), \text{ where } \hat{1} = \frac{4GM}{\mathbf{p}_f \cdot \mathbf{p}_i} (2E - m) \quad (\text{B } 1)$$

and demonstrated its gauge invariance. Below, we calculate the second term in the scattering amplitude, M_2 , in the Kerr-Schild gauge. We find the real part to be

$$M_2 = \frac{2G^2 M^2}{\hbar^2} \bar{u}_s(\mathbf{p}_f) (4E_0 - m) + \frac{4(E_0 - m)(4E^2 - m^2)}{\hbar^2 (\mathbf{p}_i + \mathbf{p}_f)^2} (1 - j \sin(\theta = 2)) u_r(\mathbf{p}_i) \quad (\text{B } 2)$$

which yields a second-order contribution to the cross section given by (17). As in the Coulomb case, the imaginary part of the scattering amplitude contains a divergent term, but the resulting polarization is finite at first-order.

The second order scattering amplitude, $M_2 = \bar{u}_s(\mathbf{p}_f) \hat{\Lambda}_2 u_r(\mathbf{p}_i)$, is defined by

$$\hat{\Lambda}_2 = \int \frac{d^3 k}{(2\pi)^3} B(\mathbf{p}_f; \mathbf{k}) \frac{\mathbb{K} + m}{k^2 - m^2 + i} B(\mathbf{k}; \mathbf{p}_i); \quad (\text{B } 3)$$

where

$$B(\mathbf{p}_2; \mathbf{p}_1) = \frac{2GM}{\hbar^2} (4E_0 - \mathbb{K} - \mathbb{K}) - \frac{4GM}{\hbar^4} (\mathbf{p}_2^2 - \mathbf{p}_1^2) (\mathbb{K} - \mathbb{K}) + \frac{i^2 GM}{\hbar^3} (\mathbf{p}_2^2 - \mathbf{p}_1^2)_0 - 2E (\mathbb{K} - \mathbb{K}); \quad (\text{B } 4)$$

and $\mathbf{q} = \mathbf{p}_2 - \mathbf{p}_1$. Our task is made easier by splitting the calculation into several parts, so that

$$B(\mathbf{p}_2; \mathbf{p}_1) = c_1 \hat{T}_1(\mathbf{p}_2; \mathbf{p}_1) + c_2 \hat{T}_2(\mathbf{p}_2; \mathbf{p}_1) + ic_3 \hat{T}_3(\mathbf{p}_2; \mathbf{p}_1); \quad (\text{B } 5)$$

where

$$\begin{aligned} (1) \quad c_1 &= 2GM; & \hat{T}_1(\mathbf{p}_2; \mathbf{p}_1) &= \frac{(4E_0 - \mathbb{K} - \mathbb{K})}{\hbar^2}; \\ (2) \quad c_2 &= 4GM; & \hat{T}_2(\mathbf{p}_2; \mathbf{p}_1) &= \frac{(\mathbf{p}_2^2 - \mathbf{p}_1^2) (\mathbb{K} - \mathbb{K})}{\hbar^4}; \\ (3) \quad ic_3 &= i^2 GM; & \hat{T}_3(\mathbf{p}_2; \mathbf{p}_1) &= \frac{(\mathbf{p}_2^2 - \mathbf{p}_1^2)_0 - 2E (\mathbb{K} - \mathbb{K})}{\hbar^3}; \end{aligned} \quad (\text{B } 6)$$

We now consider each pair of terms in (B 3) in turn, and wherever possible employ the simplification that $\mathbb{K} u_r(\mathbf{p}_i) = m u_r(\mathbf{p}_i)$ and $\bar{u}_s(\mathbf{p}_f) \mathbb{K} = \bar{u}_s(\mathbf{p}_f) m$.

First, let us consider term (2×2) , to illustrate a method for evaluating these integrals.

$$(2 \times 2) = c_2^2 \int \frac{d^3 k}{(2\pi)^3} \frac{(k^2 - \mathbf{p}^2)^2 (\mathbb{K} - m)}{\mathbf{p}_f^4 \mathbf{k} \mathbf{p}_i^4}; \quad (\text{B } 7)$$

We start by defining $Q = (p_f - p_i)/2$, $R = (p_i + p_f)/2$ and moving to the centre of mass frame, where the 1 axis is along R and the 3 axis is along Q . Then

$$\begin{aligned} k &= k + R; \\ \mathbf{k} &= \mathbf{k} + \mathbf{R} - E_0; \\ k^2 - p^2 &= k^2 - Q^2 + 2R \cdot k: \end{aligned} \quad (B8)$$

Next, we employ spheroidal coordinates, u, v, ϕ , so

$$\begin{aligned} k_1 &= \rho \sinh u \sin v \cos \phi; \\ k_2 &= \rho \sinh u \sin v \sin \phi; \\ k_3 &= \rho \cosh u \cos v: \end{aligned} \quad (B9)$$

With these coordinates the measure of integration is

$$d^3k = \rho^3 \sinh u \sin v (\sinh^2 u + \sin^2 v) du dv d\phi \quad (B10)$$

and the important quantities in the integral become

$$\begin{aligned} \mathbf{k} \cdot \mathbf{p}_2 \mathbf{k} \cdot \mathbf{p}_1 &= \mathbf{k} \cdot \mathbf{Q} \mathbf{k} + Q^2 = \rho^2 (\sinh^2 u + \sin^2 v) \\ k^2 - Q^2 &= \rho^2 (\sinh^2 u - \sin^2 v): \end{aligned} \quad (B11)$$

With these replacements, $\mathbf{k} \cdot \mathbf{m} = \mathbf{k} \cdot \mathbf{E}_0 - \mathbf{m} \cdot \mathbf{E}_0$. This has only a spatial component, so will couple to the odd part $R \cdot k$ of the rest of the integral. Therefore

$$\begin{aligned} (2 \times 2) &= c_2^2 \int \frac{d^3k}{(2\pi)^3} \frac{4(k^2 - Q^2)(R \cdot k)(\mathbf{k} \cdot \mathbf{E}_0)}{\mathbf{k} \cdot \mathbf{Q} \mathbf{k} + Q^2} \\ &= \frac{c_2^2 (\mathbf{m} \cdot \mathbf{E}_0)}{2 \int \rho^2} \int du dv \frac{\sinh^3 u \sin^3 v (\sinh^2 u - \sin^2 v)}{(\sinh^2 u + \sin^2 v)^3}: \end{aligned} \quad (B12)$$

The integral evaluates to $\int = 16$, and the result is

$$(2 \times 2) = \frac{2G^2 M^2}{\mathbf{p}_f \cdot \mathbf{p}_i} (\mathbf{m} \cdot \mathbf{E}_0): \quad (B13)$$

Similar techniques can be used to evaluate terms (3×3) , and $(1 \times 2) + (2 \times 1)$. We find

$$(3 \times 3) = \frac{2G^2 M^2}{2\mathbf{p}_f \cdot \mathbf{p}_i} (\mathbf{m} \cdot 7\mathbf{E}_0); \quad (B14)$$

$$(1 \times 2) + (2 \times 1) = \frac{2G^2 M^2}{2\mathbf{p}_f \cdot \mathbf{p}_i} (9\mathbf{E}_0 \cdot 5\mathbf{m}): \quad (B15)$$

The other cross terms, (1×3) and (2×3) , can be shown to be zero by symmetry considerations. The remaining term, (1×1) , has two parts: an integral which is tractable using the above techniques, and an integral with a pole at $|\mathbf{k}| = |\mathbf{p}|$ that is familiar from the second-order Coulomb calculation of Dalitz [21]. Explicitly,

$$(1 \times 1) = -2^2 G^2 M^2 \frac{(m - 2E_0)}{|\mathbf{p}_f - \mathbf{p}_i|} + (2E_0 - m)^2 (m + E_0) (I =^3) + (4E^2 - m^2) (E_0 - m) (J =^3) \quad (\text{B16})$$

where I and J are defined in terms of a low-frequency cut-off as

$$I = \frac{\int d^3k}{\int [(k - p_f)^2 + \epsilon^2][(k - p_i)^2 + \epsilon^2](k^2 - \epsilon^2 + i\epsilon)} \\ \frac{(\mathbf{p}_i + \mathbf{p}_f)_x}{2} J = \frac{\int k_x d^3k}{[(k - p_f)^2 + \epsilon^2][(k - p_i)^2 + \epsilon^2](k^2 - \epsilon^2 + i\epsilon)}: \quad (\text{B17})$$

To lowest order in ϵ these integrals evaluate to (see Itzykson and Zuber [41])

$$I = \frac{i^2}{2p^3 \sin^2(\epsilon/2)} \ln \frac{2p \sin(\epsilon/2)}{j} \\ J = \sec^2(\epsilon/2) I + \frac{3}{4p^3 \cos^2(\epsilon/2)} (1 - \csc(\epsilon/2)) \frac{i^2}{2p^3 \cos^2(\epsilon/2)} \ln(\epsilon/2p) \\ I - J = \frac{3}{4p^3 \cos^2(\epsilon/2)} (\csc(\epsilon/2) - 1) + \frac{i^2}{4p^3 \cos^2(\epsilon/2)} \ln(\sin^2(\epsilon/2)): \quad (\text{B18})$$

The imaginary parts of I and J diverge as $\epsilon \rightarrow 0$. However we note that the difference $I - J$ is finite. We can rewrite the I and J parts of (1×1) as

$$2I (2E^2 - m^2) (2E_0 - m) + (I - J) (4E^2 - m^2) (m - E_0): \quad (\text{B19})$$

The $2E_0 - m$ associated with the I term ensures that this term does not contribute to the polarization at first order, as we see below.

The result of summing (B13), (B14), (B15) and (B16) is

$$\hat{\alpha}_2 = \frac{2G^2 M^2}{|\mathbf{p}_f - \mathbf{p}_i|} (4E_0 - m) + \frac{4(E_0 - m)(4E^2 - m^2)}{|\mathbf{p}_i + \mathbf{p}_f|^2} (1 - \sin(\epsilon/2)) \\ + i \frac{G^2 M^2 (4E^2 - m^2) \ln(\sin^2(\epsilon/2))}{2p^3 \cos^2(\epsilon/2)} (m - E_0) + i \ln(2E_0 - m): \quad (\text{B20})$$

The second order contribution to the scattering cross section is

$$\frac{d}{d\Omega_2} = \frac{m^2}{2} \frac{1}{2} \text{Tr} \left[\frac{\not{\mathbf{p}}_i + m}{2m} \not{\Delta}_2 \frac{\not{\mathbf{p}}_f + m}{2m} \right] + \text{Tr} \left[\frac{\not{\mathbf{p}}_i + m}{2m} \not{\Delta}_1 \frac{\not{\mathbf{p}}_f + m}{2m} \right]; \quad (\text{B21})$$

where $\hat{\Delta} = \hat{\gamma}_0 \hat{y} \hat{\gamma}_0$. After employing the appropriate gamma matrix trace theorems, this evaluates to (17). The imaginary part of (B 20) does not contribute to the total unpolarized scattering cross section, but it does contribute to the net polarization. The polarized cross section in direction \hat{s} is given by

$$\begin{aligned} \frac{d}{d} \bigg|_{\text{pol}} &= \frac{1}{2} \frac{1}{16} \text{Tr} \left[\hat{G}_1 \hat{G}_{i2} \hat{G}_f \right] + \text{Tr} \left[\hat{G}_2 \hat{G}_{i1} \hat{G}_f \right] \\ &= \frac{2G^3 M^3 E m}{2 \hat{p}_f \hat{p}_f^2} (4E^2 - m^2) \text{Im} (I - J) \mathcal{B}(\hat{p}_f, \hat{p}_f): \end{aligned} \quad (\text{B } 22)$$

Here we have made use of the result

$$\text{Tr} f_5 \mathbf{a} \mathbf{b} \mathbf{c} \mathbf{d} g = 4i \mathbf{a} \mathbf{b} \mathbf{c} \mathbf{d} ; \quad (\text{B } 23)$$

where χ_{ij} is antisymmetric under exchange of any pair of indices. The fraction of polarized flux P is found by dividing polarized flux (B22) by the unpolarized flux at first order (16) to obtain result (18).

- [1] R. A. M atzner, J. M ath. Phys. 9, 163 (1968).
- [2] R. Fabbri, Phys. Rev. D 12, 933 (1975).
- [3] P. C. Peters, Phys. Rev. D 13, 775 (1976).
- [4] W. K. de Logi and S. J. K ovacs, Phys. Rev. D 16, 237 (1977).
- [5] N. G. Sanchez, J. M ath. Phys. 17, 688 (1976).
- [6] N. G. Sanchez, Phys. Rev. D 16, 937 (1977).
- [7] N. G. Sanchez, Phys. Rev. D 18, 1030 (1978).
- [8] N. G. Sanchez, Phys. Rev. D 18, 1798 (1978).
- [9] T. R. Zhang and C. D eW itt-M orette, Phys. Rev. Lett. 52, 2313 (1984).
- [10] R. A. M atzner, C. D eW itt-M orette, B. Nelson, and T. R. Zhang, Phys. Rev. D 31, 1869 (1985).
- [11] P. Anninos, C. D eW itt-M orette, R. A. M atzner, P. Y ioutas, and T. R. Zhang, Phys. Rev. D 46, 4477 (1992).
- [12] N. Andersson, Phys. Rev. D 52, 1808 (1995).
- [13] N. Andersson and B. P. Jensen, *arxiv* (2001), gr-qc/0011025.

- [14] C . J . L . D oran and A . N . Lasenby, *Phys. Rev. D* 66, 024006 (2002).
- [15] S . Chandrasekhar, *The Mathematical Theory of Black Holes*, International Series of Monographs on Physics (Oxford University Press, New York, 1983).
- [16] J . A . H . F utterman, F . A . H andler, and R . A . M atzner, *Scattering from Black Holes* (Cambridge University Press, 1988).
- [17] V . P . Frolov and I . D . Novikov, *Black hole physics: Basic concepts and new developments* (Kluwer Academic Publishers, Dordrecht, 1998).
- [18] W . G . Unruh, *Phys. Rev. D* 14, 3251 (1976).
- [19] C . Darwin, *Proc. R. Soc. Lond. A* 249, 180 (1959).
- [20] P . A . Collins, R . Debourgo, and R . M . Williams, *J. Phys. A* 6, 161 (1973).
- [21] R . H . Dalitz, *Royal Society of London Proceedings Series A* 206, 509 (1951).
- [22] K . W . Ford and J . A . Wheeler, *Annals of Physics* 7, 259 (1959).
- [23] M . Rose, *Relativistic Electron Theory* (John Wiley & Sons, 1961).
- [24] N . F . Mott and H . S . W . Massey, *The Theory of Atomic Collisions* (Oxford University Press, London, 1965).
- [25] K . Martel and E . Poisson, *Am. J. Phys.* 69, 476 (2001).
- [26] N . D . Birrell and P . C . W . Davies, *Quantum Fields in Curved Space* (Cambridge University Press, 1982).
- [27] A . N . Lasenby, C . J . L . D oran, J . Pritchard, A . Caceres, and S . R . Dolan, *Phys. Rev. D* 72, 105014 (2005).
- [28] M . Nakahara, *Geometry, Topology and Physics* (Adam Hilger, Bristol, 1990).
- [29] E . W . Leaver, *J. Math. Phys.* 27, 1238 (1986).
- [30] S . M ano, H . Suzuki, and E . Takasugi, *Prog. Theor. Phys.* 96, 549 (1996).
- [31] A . N . Lasenby, C . J . L . D oran, and S . F . Gull, *Phil. Trans. R. Soc. Lond. A* 356, 487 (1998).
- [32] N . Andersson and K . E . Thylwe, *Class. Quantum Grav.* 11, 2991 (1994).
- [33] T . Y . W u and T . Ohmura, *Quantum Theory of Scattering* (Prentice Hall, 1962).
- [34] D . R . Yennie, D . G . Ravenhall, and R . N . Wilson, *Physical Review* 95, 500 (1954).
- [35] A . A . Starobinskii and S . M . Churilov, *Zh. Eksp. Teor. Fiz.* 65, 3 (1973).
- [36] C . J . L . D oran, A . N . Lasenby, S . R . Dolan, and I . Hinder, *Phys. Rev. D* 71, 124020 (2005).
- [37] N . Arkani-Hamed, S . Dimopoulos, and G . Dvali, *Phys. Lett. B* 429, 263 (1998).
- [38] P . Kanti, *Int. J. Mod. Phys. A* 19, 4899 (2004).

- [39] K. G. Lampridakis and N. Andersson, *Class. Quantum Grav.* 18, 1939 (2001).
- [40] W. Unruh, *Phys. Rev. Lett.* 31, 1265 (1973).
- [41] C. Itzykson and J.-B. Zuber, *Quantum Field Theory* (McGraw-Hill, New York, 1980).